Characterization and in vivo toxicological evaluation of multi-walled carbon nanotubes: a low dose repeated intratracheal administrations study

Guilherme Borges Bubols
Federal University of Rio Grande do Sul: Universidade Federal do Rio Grande do Sul
Marcelo Dutra Arbo
Federal University of Rio Grande do Sul: Universidade Federal do Rio Grande do Sul
Caroline Portela Peruzzi
Federal University of Rio Grande do Sul: Universidade Federal do Rio Grande do Sul
Larissa Vivan Cestonaro
Federal University of Rio Grande do Sul: Universidade Federal do Rio Grande do Sul
Louise Figueiredo Altknecht
Federal University of Rio Grande do Sul: Universidade Federal do Rio Grande do Sul
Nuryan Fão
Federal University of Rio Grande do Sul: Universidade Federal do Rio Grande do Sul
Gabriela Göethel
Federal University of Rio Grande do Sul: Universidade Federal do Rio Grande do Sul
Sabrina Nunes Nascimento
Federal University of Rio Grande do Sul: Universidade Federal do Rio Grande do Sul
Karina Paese
Federal University of Rio Grande do Sul: Universidade Federal do Rio Grande do Sul
Marta Gonçalves Amaral
Federal University of Pelotas: Universidade Federal de Pelotas
Carlos Pérez Bergmann
Federal University of Rio Grande do Sul: Universidade Federal do Rio Grande do Sul
Adriana Raffin Pohlmann
Federal University of Rio Grande do Sul: Universidade Federal do Rio Grande do Sul
Silvia Stanisçuaski Guterres
Federal University of Rio Grande do Sul: Universidade Federal do Rio Grande do Sul
Solange Cristina Garcia (✉ solangecgarcia88@gmail.com)
Federal University of Rio Grande do Sul: Universidade Federal do Rio Grande do Sul
https://orcid.org/0000-0003-3752-5751

Research Article

Keywords: nanotoxicology, lung toxicity, rat, NM-401, NM-403, MWCNT

Posted Date: August 22nd, 2022

DOI: https://doi.org/10.21203/rs.3.rs-1865074/v1

Abstract

This study characterized and investigated the toxicity of two multi-walled carbon nanotubes (MWCNT) NM-401 and NM-403 at 60 and 180 µg after four repeated intratracheal instillations; follow-up times were 3, 7, 30 and 90 days after the last instillation. NM-401 was needle-like, long, and thick, while NM-403 was entangled, short and thin. Both MWCNT types induced transient pulmonary and systemic alterations in renal function and oxidative lipid damage markers in recent times. Animals showed general toxicity in the immediate times after exposures, in addition to increased pulmonary LDH release at day 3. In further times, decreased liver and kidney relative weights were noted at higher MWCNT doses. Lung histological damages included pulmonary fibrosis, for both MWCNT types, similarly to asbestos; single liver and kidney histological alterations were present. Repeated instillations led to persistent pulmonary damage at low doses and possibly the extrapulmonary effects may be associated with the consecutive exposures.

1. Introduction

Nanotechnology has been expanding rapidly and in this process has promoted the development and commercialization of nanomaterials for a wide range of industrial applications. Among nanomaterials, carbon nanotubes (CNT) stand out as a result of properties such as durability, high tensile strength, flexibility, and light weight, for instance, all of which are attractive to technological segments considering the potential to develop materials with improved electrical conductivity, optical transmission, gas adsorption, and more (Demczyk 2002; Jensen et al. 2015).

Carbon nanotubes are carbon allotropes composed of cylindrical graphene structures that are divided as single-wall carbon nanotubes (SWCNT) or as concentrical graphene structures named multi-wall carbon nanotubes (MWCNT) (Iijima 1991). According to industrial estimates, CNT global production ranged from 520 to 3,000 tons in 2014, from which the MWCNT market is regarded by far as the most abundant, compared to SWCNT production numbers (Jensen et al. 2015).

MWCNT have been brought into attention due to their promising physicochemical properties to improve the development of numerous available products. On the other side, manufactured MWCNT still raise concerns about safety, especially considering the occupational and environmental hazards that such nanomaterials could represent due to industrial waste. Nanotoxicity studies become of great relevance to determine their safety, especially following pulmonary exposures, which are important routes of exposures in occupational settings as well as environmental exposures (Oberdörster et al. 2015). Some features of CNT may contribute to toxicity such as tube diameters in the nanometric scale, high length/diameter aspect ratio or fiber-like shapes and the biopersistent graphitic carbon structures (Donaldson et al. 2006).

Considering the variety of carbon nanotubes regarding size, shapes, chemical composition, impurities and surface functionalization, there is still need to understand how these differences influence MWCNT toxicity (Liu et al. 2013; Poulsen et al. 2015; Poulsen et al. 2017). Most studies have focused on

investigating lung inflammation and fibrosis following inhalation, intratracheal instillation or aspiration exposures (Ma-Hock et al. 2009; Pauluhn et al. 2010; Porter et al. 2010; Wang et al. 2011), while some research is found on genotoxicity (Dong and Ma 2015; Hadrup et al. 2017), another possibly associated harmful effect for some compounds. Since most intratracheal studies are based on single acute administrations, there is need for repeated instillation schemes as well as assessing different post-exposure times to better understand the effects of MWCNT, and including asbestos fibers as a study group for comparability. Further data are still required on more carbon nanotubes to address the individual pulmonary and extrapulmonary toxicities, since extrapolation of toxicity based on physicochemical properties is not currently completely established. Thus, the objective of the present study was to characterize and investigate the pulmonary and systemic toxicity of two manufactured MWCNT after repeated intratracheal exposures in rats and in different post-exposure time points.

2. Materials And Methods

2.1. MWCNT preparation

Two pristine MWCNT NM-401 and NM-403 from the OECD Working Party on Manufactured Nanomaterials were kindly donated by the European Union Joint Research Centre (Ispra, Italy) and herein tested. These MWCNT were produced by catalytic chemical vapour deposition and originated from one respective batch of commercially manufactured MWCNT. As a reference material, asbestos crocidolite (CAS# 12001-28-4) was purchased from SPI Supplies Division of Structure Probe, Inc. (West Chester, PA, USA). Both carbon nanomaterials and crocidolite were dispersed according to the ENPRA dispersion protocol (Jensen 2014) in which the dispersion medium was modified. Stock solutions were prepared (2.56 mg/ml) in 0.1% polysorbate 80 in Milli-Q water and under continuous cooling in ice-water. The MWCNTs were dispersed by sonication with Branson S-450D 400 W, 20 kHz (Branson Ultrasonics Corp., Danbury, CT, USA) equipped with a 13 mm disruptor horn, previously adjusted to operate at a 10% amplitude during 16 minutes. Subsequently, 0.45 mg/ml and 0.15 mg/ml concentrations were obtained from the stock solution in order to be administered in the animals.

2.2. Physicochemical characterization of the MWCNT

The MWCNT were characterized in the dispersion medium or as bulk materials according to the following techniques. Transmission electron microscopy (TEM) analysis was performed to evaluate nanotube morphology and structure. Stock solutions from both nanomaterials were prepared and diluted concentrations (0.32 and 0.08 mg/ml) were deosited on a specimen grid (Formvar-Carbon support film, Electron Microscopy Sciences). Samples were analyzed and images were obtained using a transmission electron microscope (TEM; JEM 1200 Exll, Japan) operating at 80 kV at Centro de Microscopia e Microanálise (CMM/UFRGS).

Moreover, Raman spectroscopy data on carbon structure were obtained using inVia Raman microscope (Renishaw, Gloucestershire, UK). The scattering spectra were measured with an excitation wavelength of

532nm and in the region of 100 to 3200 cm^{-1} with following settings: potency 5, time 10s, and number of acquisitions 2.

The nanometric population was analyzed by dynamic light scattering (DLS) in order to determine hydrodynamic diameter distribution. As previously described, the dispersion state was evaluated by the average intensity-derived spherical equivalent hydrodynamic diameter (Jackson et al. 2015).

Hydrodynamic diameter measurements were carried out according to Jensen (2015). Briefly, MWCNT at 0.45 mg/ml and 0.15 mg/ml concentrations were prepared from stock concentration, filtered through 0.12 µm membranes and placed in 1 ml (10 × 10 × 45 mm) disposable polystyrene cuvettes for measurements at 25ºC. In order to calculate the spherical equivalent hydrodynamic size of MWCNT, 2.020 and 2.000 were adopted as refractive (R_i) and absorption indices (R_a), respectively, and the standard optical properties of H_2O as dispersant was used. The equipment was set to perform 10 repeated reads with no pause between reads and all measurement conditions were automatic for position, laser attenuation and number of runs and sub-runs. Additionally, a stability study of the dispersions was conducted, in which samples were sonicated and analyzed at 0, 60, 120, and 180 minutes after preparation. Data records were assessed by intensity and collected using the software Zetasizer 7.11 fitting the correlation data by a multiple exponential (CONTIN method). Hydrodynamic diameter of the preparations were determined using a zetasizer (Nano-ZS ZEN 3600 model®, Malvern, UK).

2.3. Animal experiments

Sprague Dawley female rats weighing approximately 200g were purchased from CEMIB/UNICAMP and housed in the local facility at UFRGS. Animals were adapted for 15 days in the local institution, kept in polypropylene boxes with sawdust bedding (41 × 34 × 16 cm), 4 animals per box, and maintained at 22 ± 2°C in 12/12h light/dark cycles (7 am – 7 pm) receiving standard food and water *ad libitum*. The animals were looked after in accordance with the Guide for the Care and Use of Laboratory Animals (NRC 2011) and following the legal requirements and local guidelines for the welfare and use of animals. The study was approved by the local Ethics Committee in Animal Use (CEUA UFRGS) under permit number 29957.

2.4. Experimental protocol

Animals were randomly distributed into six groups (n = 8 animals per group): control receiving polysorbate 80 (PS80, 0.1%), asbestos crocidolite (ASB, 180 µg), NM-401 low dose (LD401, 60 µg) and NM-401 high dose (HD401, 180 µg), as well as NM-403 low dose (LD403, 60 µg) and NM-403 high dose (HD403, 180 µg). Eight- to nine-weeks-old rats were submitted to repeated administrations by intratracheal instillations under 4% isoflurane anesthesia at day 1, day 9, day 17 and day 25. A scheme of the experimental protocol is shown in Fig. 1. Rats were submitted to the insertion of a catheter in the trachea, and the process was monitored by a sensitive pressure transducer (pneutachymeter), which aimed to assure the correct insertion prior to administrations. Instillation of 100 µl was immediately followed by 200 µl of air in the same syringe. MWCNT groups received in total four instillations of 15 µg

in low doses (cumulative dose 60 µg/rat) or 45 µg in high doses (cumulative dose 180 µg/rat). Doses were chosen from previous studies and the highest dose tested corresponded to the equivalent of the limit of human exposure established by NIOSH of 1 µg MWCNT/m^3 (NIOSH 2013; Gaté et al. 2019). Animals from each post-exposures times presented the following mean weights at the first instillation: 3 days (206.17 ± 3.73 g), 7 days (268.83 ± 4.02 g), 30 days (283.29 ± 3.23 g) and 90 days (248.83 ± 3.11 g). During and after the repeated intratracheal exposures, animals' weights were recorded until the euthanasia in different time points (3, 7, 30 and 90 days after the last exposure).

2.5. Collection of biological samples

Animals were euthanized under intraperitoneal ketamine (10%) and xylazin (2%) anesthesia by exsanguination. Whole blood was collected with heparinized syringes from the inferior vena cava and was immediately transferred to K_2EDTA and lithium heparin Vacutainer tubes (BD Diagnostics, Plymouth, UK). Aliquots from blood-EDTA were separated for hematological analysis. EDTA tubes were then centrifuged (1500 g for 10 min) and plasma-EDTA was used for MDA determination, while red blood cells (RBC) were used for GSH quantification. Whole blood-heparin was used to determine ALA-D activity, and after centrifugation, plasma-heparin was used to determine biochemical analytes.

Furthermore, lungs, heart, liver, kidneys and spleen were excised, washed with PBS saline solution, and weighed. The collected tissues were sectioned and transferred to cryotubes and stored at -80°C. Right lung caudal lobes, left lateral liver lobes, left kidneys and regular portions of spleens and hearts were separated for histopathological analysis being immediately fixed in 10% neutral buffered formalin solution. After lungs and trachea were separated from adjacent tissues and weighed, bronco-alveolar lavage fluid (BALF) was collected. Right lung lobes (cranial, median and accessory) were isolated, sectioned, and then stored at -80°C, while the caudal lobe bronchus was first reversibly tied throughout BALF collection, and thereafter untied, infused with and immersed in 10% neutral buffered formalin. Subsequently, the left lung lobe was washed with 2ml ice PBS saline solution after the insertion of a catheter in the trachea, and the recovered volume was centrifuged at 800g, 4°C for 6 minutes to obtain BALF for biochemical analysis.

2.6. Relative body weight gain and relative organ weight

General toxicity data were recorded from the administrations and follow-up times by animal weights and clinical observations. Animal body weights and the weights of the collected organs were used to calculate animal relative body weight gain (%) and relative organ weights (%).

2.7. Biochemical analysis

After plasma-heparin and BALF samples were obtained, the following biochemical parameters were determined: alanine aminotransferase (ALT), aspartate aminotransferase (AST), creatinine (CRE), urea (mg/dl), alkaline phosphatase (ALP), total protein (TPT), creatine phosphokinase (CPK), lactate dehydrogenase (LDH), gamma glutamyl transpeptidase (GGT), total cholesterol (TCH), high density lipoprotein fraction (HDL), and amylase (AMY). All analytes were determined in plasma, while AST, ALT,

ALP, LDH and TPT were measured in BALF. Biochemical analysis was performed in the chemical analyzer BS-120 (Mindray, Shenzhen, China) using commercially available kits (Bioclin, Belo Horizonte, MG, Brazil). Results were compared with the available reference ranges for rats considering the same species, sex and ages (Giknis and Clifford 2006).

2.8. Oxidative stress biomarkers

Lipid peroxidation was evaluated in plasma by determining malondialdehyde (MDA) levels by high performance liquid chromatography (HPLC) using visible detector (Grotto et al. 2007). Plasma underwent alkaline hydrolysis, acid deproteinization, thiobarbituric acid derivatization and extraction with n-butanol before injection into the chromatograph (WellChrom model, Knauer, Germany) and detection at 532 nm. MDA levels were expressed as µmol/l.

GSH levels were measured by a spectrophotometric method in the erythrocytes fraction of EDTA-containing tubes. Briefly, RBC fraction was hemolyzed with Triton X-100, and then precipitated with 20% trichloroacetic acid (w/v). Samples were centrifuged and the reaction occurred when supernatants were added to 10mM 5,5'-dithio-*bis*(2-nitrobenzoic acid) (DTNB), followed by measurements at 412 nm. Results were expressed as µmol/ml of erythrocytes (Ellman 1959).

The determination of blood δ-aminolevulinate dehydratase (ALA-D) activity was carried out in whole blood with heparin, as described by Sassa (1982) with modifications. The assay measured the rate of porphobilinogen (PBG) formation as means to determine enzymatic activity from the addition of the substrate (ALA) followed by an incubation at 37°C for 1 h. The modified Ehrlich's reagent was used to measure the PBG product and absorbance was monitored at 555 nm, considering the molar absorption coefficient of the Ehrlich-PBG salt as $6.1 \times 10^4\ M^{-1}$. Enzyme activity unit (U) is defined as 1 µmol PBG formed per hour at 37°C and the ALA-D activity was expressed as U/l.

2.9. Hematological analysis

Complete blood cell counts were performed in the automated cell analyzer ABX Pentra XL 80 (Horiba, Kyoto, Japan). The analyzed parameters were red blood cell count (RBC), hemoglobin, hematocrit (PVC), mean corpuscular volume (MCV), mean corpuscular hemoglobin (MCH), mean corpuscular hemoglobin concentration (MCHC), red cell distribution width (RDW), platelet count (PLT), mean platelet volume (MPV), white blood cell count (WBC), and neutrophiles, lymphocytes, eosinophils, monocytes, and basophiles. Results were compared with available reference ranges for rats considering the same species, sex and ages.

2.10. Histopathological analysis

Lungs, heart, kidneys, liver and spleen tissues were sectioned for histopathological analysis and fixed in 10% neutral buffered formalin (pH 7.0), and then embedded in paraffin. Lungs were slowly filled with formalin solution for fixation and kept inflated by closing the bronchus before immersion in formalin. Sections of 5–6 µm thickness from each organ were placed on slides and stained with haematoxylin and eosin. Tissue slides were analyzed under light microscope.

2.11 Statistical analysis

Data were analyzed and figures created in the software GraphPad Prism version 5.01 (San Diego, CA, USA). Kolmogorov-Smirnov normality test was applied to evaluate the distribution of variables. Results were compared using ANOVA followed by Bonferroni *post hoc* test or Kruskall-Wallis with Dunn's test for multiple comparisons. For relative weight gain and comparisons between post-administration times, data were analyzed by two-way ANOVA, while one-way ANOVA was performed when comparing study groups. Results were presented as mean ± SEM and the significance level was considered when $P < 0.05$.

3. Results

3.1. Physicochemical characterization

3.1.1. Morphological characterization: Transmission electron microscopy (TEM)

MWCNT morphological characterization by TEM showed that NM-401 are needle-like straight nanotubes displaying visible walls, while NM-403 exhibited a highly bent and entangled morphology. NM-401 nanotube diameters were found to be thicker than NM-403, and NM-401 were longer than NM-403 (Fig. 2).

3.1.2. Chemical composition: Raman spectroscopy

Raman spectra of both tested carbon nanotubes are shown in Fig. 3. NM-401 Raman spectroscopic profile indicated a high G-band (graphitic band) at approximately 1580 cm^{-1}, and a low defect/disorder band or D-band (approximately 1300 cm^{-1}), when compared to NM-403. The peaks at 2700 cm^{-1} have been identified as an overtone of the previous bands (Rasmussen et al. 2014).

3.1.3. Diameter characterization: Dynamic light scattering (DLS)

Nanotube hydrodynamic diameter characterization was performed in both tested concentrations of the MWCNT dispersions. Immediately after sonication, each preparation was analyzed by repeated measurements (Fig. 4). Results indicate differences between MWCNT diameter distributions, demonstrating that NM-401 presents an intense and predominant peak in the nanometric region (Fig. 4a-b). Low concentration NM-401 displayed a peak with mean diameter ± SD of 343.2 ± 16.5 nm and intensity of 98.3 ± 1.2%, while at high concentration such NM-401 peak was 239.1 ± 12.5 nm and 97.1 ± 2.2%, respectively.

Similar to NM-401, NM-403 at low concentration presented a predominant peak (364.8 ± 52.9 nm and 86.4 ± 1.1%), but another peak with lower diameter was found (10.1 ± 0.2 nm and 11.7 ± 0.9%). The latter

peak increased in intensity in a dose-dependent manner, given that such low-diameter peak was predominant (10.2 ± 0.08 nm and 52.6 ± 3.4%) in the high concentration NM-403 dispersion, followed by a secondary peak (269.7 ± 14.8 nm and 41.0 ± 3.1%) (Fig. 4c-d). A minor signal in the micrometric region was detected in all MWCNT and concentrations tested.

In addition, Fig. 5 presents the stability study of the preparations, reflecting the dispersion behavior within a 3-hour period that corresponds to the time from preparation to administrations. The hydrodynamic diameter profiles of both MWCNT observed in Fig. 5 were maintained during the assessed time interval. NM-401 and NM-403 dispersions were similar to the repeated reads presented in Fig. 4.

3.2. Relative body weight and relative weight of organs (%)

During the four weeks of repeated exposures, and the time points until sample collection, animals showed no relevant clinical alterations. No animal mortality was observed as a result of the exposures. Animals were found to present significant loss of body weight gain for both MWCNTs tested 3 days after the instillations in relation to vehicle controls (Fig. 6). At day 7, NM-401 at the high dose was the only group in which relative body weight gain was significantly decreased, with all remaining groups not demonstrating the continuation of significant alterations. Besides, body weight gain effects did not persist in further times post exposure, as demonstrated in growth curves between groups after 30 days of repeated exposures. However, curves after 60 and 90 days of exposures indicated significant increase in weight gain in relation to PS80 and to asbestos (Fig. 6d).

Figure 7 depicts relative weights of organs in all time points evaluated, indicating that 30 days after administrations liver showed decreased relative weights in HD403 compared to PS80 (Fig. 7b). In addition, after 90 days of exposures in HD401 and HD403 groups, left kidneys presented significantly reduced relative weights in relation to PS80 (Fig. 7d). On the other hand, relative organ weights of lungs, heart, and spleen showed no statistical significance compared to the PS80 group.

In addition, time-dependent decreased liver weights for NM-403 at high dose were found after 30 and 90 days in relation to 3 days, as well as at low dose after 90 days compared to 3 days. More time-dependent decreases were found for asbestos and low dose NM-401 (Fig. 7b); decreased relative weights in left kidneys were also found in HD401 and HD403 after 90 days of exposures compared to 3 days, as well as in LD401 (Fig. 7d). Right kidneys also displayed decreased weights at further times in HD403 and LD401, similarly to left kidneys (Fig. 7c). No MWCNT groups presented alteration in lung relative weights, only decreased tissue weights in PS80 at 90 days compared to 3 days (Fig. 7a). No group differences in relative heart weights were found, but such weights decreased with time in LD401 and LD403 groups as well as asbestos (Fig. 7f). The only spleen alteration was a decrease in LD401 times compared to 3 days (Fig. 7e).

3.3. Biochemical and oxidative stress markers

Data from day 3 after administrations indicate significantly increased levels of plasma creatinine in the group that received the highest NM-401 dose, and elevation of urea levels in the high dose NM-403 group compared to vehicle controls, as shown in Fig. 8a and 8b, respectively. The mean creatinine levels were within reference values in the study groups, including the PS80 groups with increased levels, and the HD401 groups with decreased levels in further times (Fig. 8a). Besides, mean urea results were found above reference range (23.54–36.38 mg/dl) in the study groups and were found to decrease in HD403 in subsequent times (Fig. 8b). In fact, both kidney markers from MWCNT groups after day 3 presented significantly reduced levels.

According to Fig. 8c, LDH levels in BALF were significantly increased 3 days after administrations in LD403 and HD403 compared to vehicles. Data on the additional time points indicated no statistical significance relative to vehicles, despite higher mean values were obtained at days 30 and 90 after administrations, but both LD403 and HD403 at day 30 presented significantly increased LDH release compared to day 3. Further biochemical analytes determined in plasma and BALF were found not to be significantly changed in study groups (data not shown).

Table 1 summarizes the findings related to the oxidative stress blood markers determined. Malondialdehyde was found elevated 3 days after administrations at the highest NM-401 dose in comparison to PS80 and asbestos, while high dose NM-403 MDA levels were enhanced compared to asbestos. No significant alterations were observed in the remaining time points for any tested nanocompounds. Furthermore, GSH levels in the HD401 group were significantly increased at day 3 compared to PS80, and decreased in HD403 compared to asbestos. However, GSH was not changed in the subsequent times. Table 1 also demonstrates that no significant alterations were observed for ALA-D among all of the studied groups.

Table 1
Oxidative stress biomarkers measured in blood samples of the study groups

		PS80	ASB	LD401	HD401	LD403	HD403
MDA (mM)	Day 3	20.03 ± 0.90	18.89 ± 1.33	21.92 ± 2.07	31.37 ± 2.74*,##	24.79 ± 2.37	29.87 ± 3.57#
	Day 7	51.24 ± 8.34	54.92 ± 6.93	54.78 ± 7.44	52.31 ± 6.58	64.89 ± 5.26	62.79 ± 3.01
	Day 30	37.49 ± 5.54	29.05 ± 2.54	33.53 ± 1.49	36.85 ± 4.22	29.27 ± 3.19	35.39 ± 3.45
	Day 90	33.73 ± 2.00	42.36 ± 5.35	34.19 ± 2.75	32.93 ± 2.93	35.40 ± 2.15	42.36 ± 2.96
GSH (µmol/ml RBC)	Day 3	0.91 ± 0.03	1.06 ± 0.06	1.11 ± 0.06	1.22 ± 0.11*	0.76 ± 0.02#	0.70 ± 0.03##
	Day 7	0.78 ± 0.07	0.84 ± 0.05	0.79 ± 0.05	0.88 ± 0.03	0.79 ± 0.02	0.90 ± 0.10
	Day 30	0.87 ± 0.01	0.75 ± 0.07	1.03 ± 0.19	1.19 ± 0.14	1.04 ± 0.08	1.09 ± 0.09
	Day 90	0.95 ± 0.11	0.79 ± 0.08	1.04 ± 0.19	1.15 ± 0.12	1.06 ± 0.07	1.10 ± 0.10
ALA-D activity (U/L)	Day 3	1.33 ± 0.31	1.29 ± 0.21	1.61 ± 0.51	2.06 ± 0.27	1.66 ± 0.33	1.52 ± 0.21
	Day 7	2.03 ± 0.55	1.67 ± 0.18	1.88 ± 0.31	2.89 ± 0.55	1.67 ± 0.39	2.80 ± 0.58
	Day 30	2.32 ± 0.21	2.48 ± 0.27	2.69 ± 0.25	2.51 ± 0.43	2.44 ± 0.25	2.37 ± 0.36
	Day 90	3.07 ± 0.53	3.03 ± 0.47	2.62 ± 0.63	2.88 ± 0.31	2.82 ± 0.44	3.51 ± 0.30

Abbreviations: MDA: malondialdehyde, GSH: glutathione, RBC: red blood cells, ALA-D: δ-aminolevulinate dehydratase. * $P < 0.05$ compared to PS80, # $P < 0.05$ compared to ASB, ## $P < 0.01$ compared to ASB. Statistical analysis – MDA (Kruskal-Wallis/Dunn) and GSH (one-way ANOVA/Bonferroni). Data are shown as mean ± SEM (n = 6–8/group)

3.4. Hematological analysis

The findings on hematological parameters in the studied groups are shown in Supplementary Material. MCHC values were slightly above expected ranges (32.60–36.00%) exclusively at day 3 HD403 (Table 1, Supplementary Material), however such increase does not seem to present relevance. Therefore, no statistical changes of clinical significance were found in hematological parameters analyzed from complete blood counts.

3.5. Histopathological analysis

Results from the lung histology (Fig. 9) indicate bronchus-associated lymphoid tissue (BALT), alveolar septal thickening and granuloma in the alveolar, peribronchiolar and perivascular regions, in tissue sections from MWCNT and asbestos groups, as in some PS80 groups. Moreover, MWCNT and asbestos exposed animals presented consistent presence of hemorrhage points from day 3, while single cases of hemorrhage were observed in PS80 at days 3 and later at 30 and 90 days. Fibrosis was observed in MWCNT-exposed groups after day 30 in both nanotubes types and doses (Fig. 9c, 9f), but a single case was found at day 7 in LD401; fibrosis was present at 90 days after exposures in asbestos group.

Additionally, extrapulmonary tissues were unaltered at day 3. In further times, some changes were observed, according to Fig. 10, especially the presence of spleen macrophages containing dark dots at days 7, 30 and 90 in asbestos, NM-401 and NM-403. Conversely, in liver and kidneys only few occurrences of alterations were found. Single kidney alterations were observed, as shown in Fig. 10 (b, c and e), and intertubular intersticial granuloma at day 90 in LD403. In the liver, rare Kupffer cells with dark dots were found at day 7 in NM-401 (Fig. 10a) and asbestos, and a small focal granuloma in portal space in NM-403 at day 30 (Fig. 10d). No heart histological changes in MWCNT groups were found; the only finding in this tissue occurred at day 30 in one animal from asbestos group that presented dark dots in heart blood vessels, liver, kidney, and in spleen macrophages.

4. Discussion

The present study tested OECD reference manufactured materials and provided physicochemical characterization of the dispersed MWCNT to examine the pulmonary toxicity. Intratracheal administrations in nanotoxicity studies are a good strategy to ensure suitable dose control and fully internalization (Driscoll et al. 2000). Another concern in our study was to perform repeated pulmonary exposures in the animals to provide a better simulation of occupational scenarios, in addition to assessing recent and late post-exposure periods. The administered doses were chosen from previously available studies and the highest dose instilled corresponded to the limit of human exposure established by NIOSH at 1 µg MWCNT/m^3 (NIOSH 2013; Gaté et al. 2019).

Considering the high hydrophobicity of both MWCNT, the nonionic surfactant polysorbate 80 at 0.1% was incorporated in our dispersion solution to improve dispersion conditions. Kobayashi et al. (2011) reported a well-dispersed preparation of SWCNT achieved with 1% polysorbate 80 in order to be administered by intratracheal instillation in rats, and the same dispersive agent has been used in another instillation study (Reddy et al. 2012). The studied carbon nanotubes were characterized and compared to previous studies (Jackson et al. 2015; Rasmussen et al. 2014), in which dispersion solution included mouse or rat serum, while in this work serum was substituted by polysorbate 80. According to TEM micrographs, clear morphological differences were observed between the two MWCNT, consistent with previously available information (Rasmussen et al. 2014). The Raman spectra obtained from the MWCNT indicate that NM-401 has a more graphitic structure due to its higher G band and lower disorder-induced D band in comparison to NM-403, similarly to the available data (Rasmussen et al. 2014; Tailor 2018).

DLS findings indicate clear differences in both MWCNT, showing that NM-401 presents an intense peak in the nanometric region, while NM-403 analysis shows another peak at approximately 10 nm, in addition the similarly intense peak similar found in NM-401. Interestingly, the NM-403 low-sized peak was dose-dependent, suggesting that the shorter MWCNT fraction was enhanced as more amount of MWCNT was present in the dispersion, possibly due to more breaks in nanotube lengths, especially considering that NM-403 narrow diameters shown in TEM results could explain the propensity to break during sonication.

The micrometric signals detected indicate agglomeration of MWCNT, as previously reported (Wang et al. 2011; Jackson et al. 2015), occurring due to van der Waals interactions between layers of sp^2 hybridised carbons (Tailor 2018). Similar to our data, Wang et al. (2011) reported bundling effects from DLS results that showed a micrometric peak due to the hydrophobic MWCNT interactions, in addition to the major nanometric peak. Jackson et al. (2015) tested both MWCNT by DLS in a different dispersion medium and reported agglomeration. Furthermore, both MWCNT from our study maintained the same pattern of particle size distribution in either short repeated reads analysis or the stability study, demonstrating that the dispersions remained suitably stable within the hours of preparation and administrations to the animals.

Pulmonary exposure to both MWCNT indicated signs of general toxicity associated with the repeated administrations shortly after the consecutive exposures noted in animal weight curves. In further times such effect was no longer detected among groups, but subsequently after 60 and 90 days following exposures NM-exposed rats gained significantly more body weight than controls, indicating a reversion of the negative effects observed in recent post-exposure times. Recently, Knudsen et al. (2019) reported no difference in mice weight gain after single intratracheal instillation with NM-401 and NM-403 compared to controls; however, the different animal species, administrations and doses may account for these observations.

The decreased liver and kidney relative weights in MWCNT groups at late time points could be related to low blood perfusion, decreased liquid amount in the organ or cell death. Besides, a few alterations of kidney and liver histology were present in MWCNT groups, in addition to the transitory renal markers changes observed only at day 3. These results altogether could indicate kidneys and liver as secondary sites affected in the study groups. No MWCNT-related lung relative weight change was found in this study, only PS80 elicited a late decrease in relative weight. No previous organ weight data were found on both MWCNT. In a previous study after SWCNT instillation, for instance, lung weight was found increased, but the authors did not report weight records on other tissues (Kobayashi et al. 2011).

There are scarce reports on plasma biomarkers from MWCNT-exposed rats by intratracheal instillation (Kavosi et al. 2018), and to the best of our knowledge, this is the first study to report several biomarkers on both nanotubes tested, since most previous studies focused only on BALF markers or inhalation exposures (Ma-Hock 2009; Pauluhn 2010; Porter et al. 2010; Wang et al. 2011; Reddy et al. 2012; Poulsen et al. 2015; Poulsen et al. 2017). Here we showed transitory alterations in renal function 3 days after instillations, but not in further post-exposure times, while additional biomarkers demonstrated no

statistical changes. No previous report on renal markers has been found indicating similar alterations. Kavosi et al. (2018) reported that MWCNT exposure led to increased levels of liver enzymes, although the authors emphasize that SWCNT-treated mice showed a more pronounced increase in transaminases. The different MWCNT tested in our study showed no signs of liver toxicity in terms of plasma biomarkers.

In relation to LDH, numerous researches reported its levels in BALF to assess lung toxicity of several types of MWCNT, especially in inhalation studies (Pauluhn 2010; Johansson et al. 2017; Hadrup et al. 2017; Rahman et al. 2017; Gaté et al. 2019). However, for both MWCNT in this study, little has been demonstrated in the literature. We showed that BALF LDH was significantly enhanced at day 3 after instillations of both NM-401 and NM-403 in high doses, but such significance was not observed in further times. Despite the different routes of administration, our findings are consistent with a recent study reporting that LDH levels in BALF were significantly increased 3 days of a nose-only inhalation study with both NM-401 and NM-403. The authors also observed that after 30 and 180 days of follow-up after exposures to NM-401, little or no LDH increase was found, but after 90 days significant increases were found. Regarding NM-403 in further times, only slight changes were reported in LDH levels (Gaté et al. 2019).

Malondialdehyde is a biomarker of oxidative damage to lipids (Garcia et al. 2013) which was increased only 3 days after the exposures. MDA levels determined in a previous study were found to increase after intratracheal administrations of other types of MWCNT after 24 h of single-dose instillations. Similarly to our report, the increased lipid damage was found to decrease in subsequent periods evaluated, despite the authors still found some degree of lipid damage in higher doses after 3 months (Reddy et al. 2011).

GSH were also increased at day 3, only for NM-401, concomitantly to the MDA increase, which could indicate that the initiation of oxidative stress imbalance along with an expected glutathione thiol depletion started in this group during the long period of repeated instillations, and later triggered a compensatory effect aimed to increase total thiols, which were found to peak immediately after the end of administrations. Since subsequently GSH levels were not significantly altered, a normalization of previous oxidative imbalance is indicated. Current research has emphasized that the amount of glutathione produced by cells is extensively superior to the necessary to scavenge ROS and also that a small portion of glutathione is oxidized and that in most conditions the fast turnover and rapid synthesis of GSH promote the thiol supply to compensate ROS damages (Poole 2015; Boysen 2017).

This study found neither hematological alterations nor changes in ALA-D activity in the exposed animals compared to controls. The complete blood count data presented in our study were within the expected ranges, and despite the significant increase in MCHC values at 3 days post-exposures, it indicates no disturbance of clinical relevance. In a study comparing another type of multi-walled CNT and a SWCNT, the authors showed that MCHC values were increased in SWCNT, in spite of the unchanged values in the MWCNT tested (Kavosi et al. 2018).

Histological findings indicate that both MWCNT tested and crocidolite induced lung alterations in the exposed animals in recent time points, and in further time points these MWCNT changes were intensified,

including crocidolite and PS80. Both MWCNT types induced damages such as enhanced hemorrhagic foci and fibrosis. Lung histological changes after exposure to MWCNT have been previously demonstrated, especially granuloma, alveolar septa thickening as well as fibrosis. Rahman et al. (2017) reported that mice exposed to NM-401 presented mild lung collagen deposition, in addition to presence of MWCNT in bundles within the lung tissues in fibrotic foci after 90 days of exposures. Similarly to our findings, the authors also found granulomatous lesions. Moreover, Knudsen et al. (2019) demonstrated in a single instillation study in mice that NM-403 induced granuloma, while the needle-like CNTs tested such as NM-401 showed no signs of histopathological changes. Our data indicate that both types of MWCNT induced tissue damage after repeated-dose administrations.

PS80 is an approved excipient for pulmonary administration; however its presence in vehicles could be responsible for part of the histological effects noted after the exposure conditions and time points. Adding NM-401 and NM-403 to the instillation fluids, nevertheless, led to intense histological responses after 3 days of exposures and consistently thereafter. In an acute administration study, animals exposed to inhalable PS80-coated NP powder presented microhemorrhage, and these changes were associated with alteration of pulmonary surfactant caused by decreased collapse pressure (Al-Hallak et al. 2010).

In this study, the endpoint effects elicited by NM-401 and NM-403 were observed at both doses tested, suggesting no dose-dependent relation in the chosen dose range for such endpoints, or solely at the highest instilled dose, e.g. liver and kidneys, MDA and renal markers. Another remark is that for some endpoints, both nanotube types led to similar alterations, such as lung histology, animal and organ weights; on the other hand, few differences were noted between nanotubes regarding LDH release. The significant pulmonary LDH release at day 3 was found only after the short and thin NM-403 was instilled to the lungs, then LDH increased in further times for both types of nanotubes.

We tested doses within the limit of exposure recommended for carbon nanotubes (NIOSH 2013) and report systemic and pulmonary effects of the repeated instillations in rats. In this study, we observed lung damage in lower doses than previously reported in single administration or inhalation protocols (Gaté et al. 2019). The repeated exposures could explain the increased pulmonary toxicity observed, based on the longer time of accumulation in the lungs even after the normal lung clearance pathways to the pleural cavity and lymphatic system. In this context, a recent study (Hojo et al. 2022) has suggested that repeated intratracheal exposures to the well-known lung carcinogen MWNT-7 (Mitsui-7) during a two-year exposure carcinogenicity study led to different outcomes as compared to a protocol with only initial exposures. The increased carcinogenicity observed after intermittent repeated exposures could be explained by the accumulation and the higher lung burden achieved.

The effects herein reported were detected primarily in lungs, but also scarce liver and kidney alterations were found. There is increasing data on the biodistribution of carbon nanotubes indicating that, once accumulated in the lungs, MWCNT may undergo translocation to pleura and lymph nodes, and extrapulmonary tissues such as liver, kidneys and spleen (Jacobsen et al. 2017). The presence and the

effects of NM-401 and NM-403 in such distal organs are of great relevance since there is currently limited evidence of their impact in these tissues.

5. Conclusion

The early findings for both pristine MWCNT (impairment of weight gain, higher levels of kidney function biomarkers, increased lipid damage, and lung LDH release) demonstrate initial and transient injuries recently after the consecutive pulmonary low-dose exposures, since most alterations were limited to recent post-exposure times. Nonetheless, in further times, together with the consistent pulmonary fibrosis and inflammation, few alterations were observed after instillations to the test compounds, such as the liver and kidney weight decreases mostly in MWCNT high dose groups, and the scarce liver and kidney histological alterations, which highlights these tissues as possible secondary targets after repeated instillations. In conclusion, this study detected persistent lung damage at low doses after repeated MWCNT administrations, which could have enhanced the pulmonary damage by allowing a continued presence of MWCNT in lung parenchyma, hence the occurrence of local toxicity at such doses, and possible translocation to extrapulmonary organs, considering the kidney and liver discrete findings.

Declarations

Ethical Approval

The animals were looked after in accordance with the Guide for the Care and Use of Laboratory Animals (NRC 2011) and following the legal requirements and local guidelines for the welfare and use of animals. The study was approved by the local Ethics Committee in Animal Use (CEUA UFRGS) under permit number 29957.

Consent to Participate

Not applicable.

Consent to Publish

All authors read and approved the final manuscript and consent with the publication.

Author Contributions

Conceptualization: Garcia SC, Pohlmann AR, Guterres SS; Methodology: Garcia SC, Pohlmann

AR, Guterres SS; Formal analysis and investigation: Bubols GB, Arbo MD, Peruzzi CP, Cestonaro LV, Altknecht LF, Fão N, Göethel G, Nascimento SN, Paese K, Amaral MG, Bergmann CP; Writing - original draft preparation: Bubols GB; Writing - review and editing: Arbo MD, Garcia SC; Funding acquisition: Garcia SC; Resources: Garcia SC, Pohlmann AR, Guterres SS; Supervision: Garcia SC.

Funding

This work was conducted in the framework of “Fundação de Amparo à Pesquisa do Estado do Rio Grande do Sul” (Fapergs/Proex) and National Institute of Science and Technology of Pharmaceutical Nanotechnology (INCT-Nanofarma), which is supported by “Fundação de Amparo à Pesquisa do Estado de São Paulo” (Fapesp, Brazil) [grant number 14/50928-2] and Conselho Nacional de Desenvolvimento Científico e Tecnológico (CNPq, Brazil) [grant number 465687/2014-8], and NANoREG. S.C. Garcia is recipient of CNPq research fellowship.

Competing Interests

The authors have no relevant financial or non-financial interests to disclose.

Availability of data and materials

Not applicable.

References

1. Al-Hallak MHDK, Azarmi S, Sun C, Lai P, Prenner EJ, Roa WH, Löbenberg R (2010) Pulmonary Toxicity of Polysorbate-80-coated Inhalable Nanoparticles; In vitro and In vivo Evaluation. The AAPS Journal 12:294-299. https://doi.org/10.1208/s12248-010-9190-4
2. Boysen G (2017) The Glutathione Conundrum: Stoichiometric Disconnect between Its Formation and Oxidative Stress. Chem Res Toxicol 30:1113-1116. https://doi.org/10.1021/acs.chemrestox.7b00018
3. Demczyk BG, Wang YM, Cumings Y, Hetman M, Han W, Zettl A, Ritchie RO (2002) Direct mechanical measurement of the tensile strength and elastic modulus of multiwalled carbon nanotubes. Materials Science and Engineering A 334:173-178. https://doi.org/10.1016/S0921-5093(01)01807-X
4. Donaldson K, Aitken R, Tran L, Stone V, Duffin R, Forrest G, Alexander A (2006) Carbon nanotubes: A review of their properties in relation to pulmonary toxicology and workplace safety. Toxicol Sci 92:5-22. https://doi.org/10.1093/toxsci/kfj130
5. Dong J, Ma Q (2015) Advances in mechanisms and signaling pathways of carbon nanotube toxicity. Nanotoxicology 9:658-676. https://doi.org/10.3109/17435390.2015.1009187
6. Driscoll KE, Costa DL, Hatch G, Henderson R, Oberdorster G, Salem H, Schlesinger RB (2000) Intratracheal instillation as an exposure technique for the evaluation of respiratory tract toxicity: uses and limitations. Toxicol Sci 55:24-35. https://doi.org/10.1093/toxsci/55.1.24
7. Ellman GL (1959) Tissue sulfhydryl groups. Arch Biochem Biophys 82:70-77. https://doi.org/10.1016/0003-9861(59)90090-6
8. Garcia SC, Grotto D, Bulcão RP, Moro AM, Roehrs M, Valentini J, de Freitas FA, Paniz C, Bubols GB, Charão MF (2013) Evaluation of lipid damage related to pathological and physiological conditions. Drug Chem Toxicol 36:306-312. https://doi.org/10.3109/01480545.2012.720989

9. Gaté L, Knudsen KB, Seidel C, Berthing T, Chézeau L, Jacobsen NR, Valentino S, Wallin H, Bau S, Wolff H, Sébillaud S, Lorcin M, Grossmann S, Viton S, Nunge H, Darne C, Vogel U, Cosnier F (2019) Pulmonary toxicity of two different multi-walled carbon nanotubes in rat: Comparison between intratracheal instillation and inhalation exposure. Toxicol Appl Pharmacol 375:17-31. https://doi.org/10.1016/j.taap.2019.05.001
10. Giknis MLA, Clifford CB (2006) Clinical Laboratory Parameters for Crl:CD(SD) Rats. Charles River Laboratories
11. Grotto D, Santa Maria LD, Boeira S, Valentini J, Charão MF, Moro AM, Nascimento PC, Pomblum VJ, Garcia SC (2007) Rapid quantification of malondialdehyde in plasma by high performance liquid chromatography-visible detection. J Pharm Biomed Anal 43:619-624. https://doi.org/10.1016/j.jpba.2006.07.030
12. Hadrup N, Bengtson S, Jacobsen NR, Jackson P, Nocun M, Saber AT, Jensen KA, Wallin H, Vogel U (2017) Influence of dispersion medium on nanomaterial-induced pulmonary inflammation and DNA strand breaks: investigation of carbon black, carbon nanotubes and three titanium dioxide nanoparticles. Mutagenesis 32:581-597. https://doi.org/10.1093/mutage/gex042
13. Hojo M, Maeno A, Sakamoto Y, Ohnuki A, Tada Y, Yamamoto Y, Ikushima K, Inaba R, Suzuki J, Taquahashi Y, Yokota S, Kobayashi N, Ohnishi M, Goto Y, Numano T, Tsuda H, Alexander DB, Kanno J, Hirose A, Inomata A, Nakae D (2022) Two-year intermittent exposure of a multiwalled carbon nanotube by intratracheal instillation induces lung tumors and pleural mesotheliomas in F344 rats. Part Fibre Toxicol. https://10.1186/s12989-022-00478-7
14. Iijima S (1991) Helical microtubules of graphitic carbon. Nature 354:56-58. https://doi.org/10.1038/354056a0
15. Jackson P, Kling K, Jensen KA, Clausen PA, Madsen AM, Wallin H, Vogel U (2015) Characterization of genotoxic response to 15 multiwalled carbon nanotubes with variable physicochemical properties including surface functionalizations in the FE1-Muta(TM) mouse lung epithelial cell line. Environ Mol Mutagen 56:183-203. https://doi.org/10.1002/em.21922
16. Jacobsen NR, Moller P, Clausen PA, Saber AT, Micheletti C, Jensen KA, Wallin H, Vogel U (2017) Biodistribution of carbon nanotubes in animal models. Basic Clin Pharmacol Toxicol 121:30-43. https://doi.org/10.1111/bcpt.12705
17. Jensen KA (2014) The ENPRA dispersion protocol for NANoREG. Version 1.0. http://safenano.re.kr/download.do?SEQ=174. Accessed 12 March 2022
18. Jensen KA (2015) NRCWE SOP for measurement of hydrodynamic Size-Distribution and Dispersion Stability by Dynamic Light Scattering (DLS). http://portal.s2nano.org:8282/files/DLS_Protocol_nanoReg.pdf. Accessed 12 March 2022
19. Jensen KA, Bøgelund J, Jackson P, Jacobsen NR, Birkedal R, Clausen PA, Saber AT, Wallin H, Vogel UB (2015) The Danish Environmental Protection Agency. Carbon Nanotubes. Types, Products, Market, and Provisional Assessment of the Associated Risks to Man and the Environment.

Environmental Project No. 1805. https://www2.mst.dk/Udgiv/publications/2015/12/978-87-93352-98-8.pdf. Accessed 12 March 2022

20. Johansson HKL, Hansen JS, Elfving B, Lund SP, Kyjovska ZO, Loft S, Barfod KK, Jackson P, Vogel U, Hougaard KS (2017) Airway exposure to multi-walled carbon nanotubes disrupts the female reproductive cycle without affecting pregnancy outcomes in mice. Part Fibre Toxicol https://doi.org/10.1186/s12989-017-0197-1
21. Kavosi A, Hosseini Ghale Noei S, Madani S, Khalighfard S, Khodayari S, Khodayari H, Mirzaei M, Kalhori MR, Yavarian M, Alizadeh AM, Falahati M (2018) The toxicity and therapeutic effects of single-and multi-wall carbon nanotubes on mice breast cancer. Sci Rep https://doi.org/10.1038/s41598-018-26790-x
22. Knudsen KB, Berthing T, Jackson P, Poulsen SS, Mortensen A, Jacobsen NR, Skaug V, Szarek J, Hougaard KS, Wolff H, Wallin H, Vogel U (2019) Physicochemical predictors of Multi-Walled Carbon Nanotube-induced pulmonary histopathology and toxicity one year after pulmonary deposition of 11 different Multi-Walled Carbon Nanotubes in mice. Basic Clin Pharmacol Toxicol 124:211-227. https://doi.org/10.1111/bcpt.13119
23. Kobayashi N, Naya M, Mizuno K, Yamamoto K, Ema M, Nakanishi J (2011) Pulmonary and systemic responses of highly pure and well-dispersed single-wall carbon nanotubes after intratracheal instillation in rats. Inhal Toxicol 23:814-828. https://doi.org/10.3109/08958378.2011.614968
24. Liu Y, Zhao Y, Sun B, Chen C (2013) Understanding the toxicity of carbon nanotubes. Acc Chem Res 46:702-713. https://doi.org/10.1021/ar300028m
25. Ma-Hock L, Treumann S, Strauss V, Brill S, Luizi F, Mertler M, Wiench K, Gamer AO, van Ravenzwaay B, Landsiedel R (2009) Inhalation toxicity of multiwall carbon nanotubes in rats exposed for 3 months. Toxicol Sci 112:468-481. https://doi.org/10.1093/toxsci/kfp146
26. National Research Council (NRC) (2011) Environment, housing, and management. In: Guide for the care and use of laboratory animals, 8th edn. National Academies Press, Washington (DC). https://www.ncbi.nlm.nih.gov/books/NBK54046/. Accessed 12 March 2022
27. NIOSH (2013) Current Intelligence Bulletin 65: Occupational Exposure to Carbon Nanotubes and Nanofibers. DHHS (NIOSH), Publication number 2013-145. https://www.cdc.gov/niosh/docs/2013-145/default.html. Accessed 12 March 2022
28. Oberdörster G, Castranova V, Asgharian B, Sayre P (2015) Inhalation Exposure to Carbon Nanotubes (CNT) and Carbon Nanofibers (CNF): Methodology and Dosimetry. J Toxicol Environ Health B Crit Rev 18:121-212. https://doi.org/10.1080/10937404.2015.1051611
29. Pauluhn J (2010) Subchronic 13-week inhalation exposure of rats to multiwalled carbon nanotubes: Toxic effects are determined by density of agglomerate structures, not fibrillar structures. Toxicol Sci 113:226-242. https://doi.org/10.1093/toxsci/kfp247
30. Poole LB (2015) The basics of thiols and cysteines in redox biology and chemistry. Free Radic Biol Med 80:148-157. https://doi.org/10.1016/j.freeradbiomed.2014.11.013

31. Porter DW, Hubbs AF, Mercer RR, Wu N, Wolfarth MG, Sriram K, Leonard S, Battelli L, Schwegler-Berry D, Friend S, Andrew M, Chen BT, Tsuruoka S, Endo M, Castranova V (2010) Mouse pulmonary dose- and time course-responses induced by exposure to multi-walled carbon nanotubes. Toxicology 269:136-147. https://doi.org/10.1016/j.tox.2009.10.017
32. Poulsen SS, Saber AT, Williams A, Andersen O, Købler C, Atluri R, Pozzebon ME, Mucelli SP, Simion M, Rickerby D, Mortensen A, Jackson P, Kyjovska ZO, Mølhave K, Jacobsen NR, Jensen KA, Yauk CL, Wallin H, Halappanavar S, Vogel U (2015) MWCNTs of different physicochemical properties cause similar inflammatory responses, but differences in transcriptional and histological markers of fibrosis in mouse lungs. Toxicol Appl Pharmacol 284:16-32. https://doi.org/10.1016/j.taap.2014.12.011
33. Poulsen SS, Knudsen KB, Jackson P, Weydahl IE, Saber AT, Wallin H, Vogel U (2017) Multi-walled carbon nanotube-physicochemical properties predict the systemic acute phase response following pulmonary exposure in mice. PLoS One. https://doi.org/10.1371/journal.pone.0174167
34. Rahman L, Jacobsen NR, Aziz SA, Wu D, Williams A, Yauk CL, White P, Wallin H, Vogel U, Halappanavar S (2017) Multi-walled carbon nanotube-induced genotoxic, inflammatory and pro-fibrotic responses in mice: Investigating the mechanisms of pulmonary carcinogenesis. Mutat Res 823:28-44. https://doi.org/10.1016/j.mrgentox.2017.08.005
35. Rasmussen K, Mast J, De Temmerman P, Verleysen E, Waegeneers N, Van Steen F, Pizzolon J, De Temmerman L, Van Doren E, Jensen K, Birkedal R, Clausen P, Kembouche Y, Thieriet N, Spalla O, Giuot C, Rousset D, Witschger O, Bau S, Bianchi B, Shivachev B, Dimowa L, Nikolova R, Nihtianova D, Tarassov M, Petrov O, Bakardjieva S, Motzkus C, Labarraque G, Oster C, Cotogno G, Gaillard C (2014) Multi-walled Carbon Nanotubes, NM-400, NM-401, NM-402, NM-403: Characterization and Physico-Chemical Properties. Publications Office of the European Union. https://publications.jrc.ec.europa.eu/repository/handle/JRC91205. Accessed 12 March 2022
36. Reddy AR, Rao MV, Krishna DR, Himabindu V, Reddy YN (2011) Evaluation of oxidative stress and anti-oxidant status in rat serum following exposure of carbon nanotubes. Regul Toxicol Pharmacol 59:251-257. https://doi.org/10.1016/j.yrtph.2010.10.007
37. Reddy AR, Reddy YN, Krishna DR, Himabindu V (2012) Pulmonary toxicity assessment of multiwalled carbon nanotubes in rats following intratracheal instillation. Environ Toxicol 27:211-219. https://doi.org/10.1002/tox.20632
38. Sassa S (1982) δ-Aminolevulinic acid dehydratase assay. Enzyme 28:133-145. https://doi.org/10.1159/000459097
39. Tailor PM, Wheatley RJ, Besley NA (2018) Simulation of the Raman spectroscopy of multi-layered carbon nanomaterials. Phys Chem Chem Phys 20:28001-28010. https://doi.org/10.1039/c8cp05908j
40. Wang X, Katwa P, Podila R, Chen P, Ke PC, Rao AM, Walters DM, Wingard CJ, Brown JM (2011) Multi-walled carbon nanotube instillation impairs pulmonary function in C57BL/6 mice. Part Fibre Toxicol. https://doi.org/10.1186/1743-8977-8-24

Figures

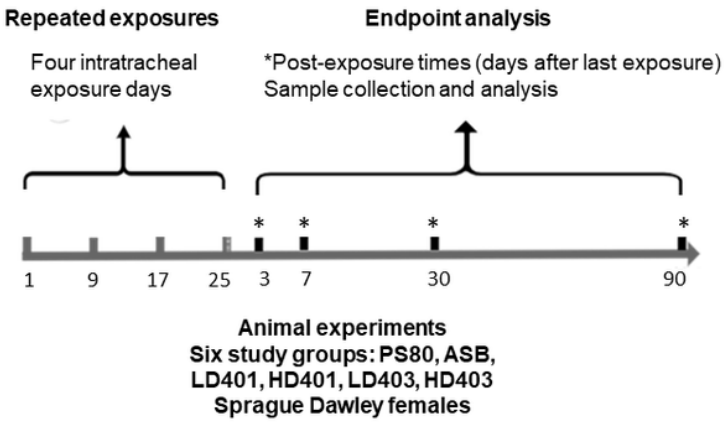

Figure 1

Scheme of the experimental protocol, representing the four consecutive intratracheal instillations of nanomaterials and the experiments on four different post-exposure times (3, 7, 30 and 90 days) after the last instillation. Study groups (n=6-8 each) are indicated as PS80: polysorbate 80 (0.1%) vehicle, ASB: asbestos crocidolite, LD401 and HD401: low dose and high dose NM-401, respectively, LD403 and HD403: low dose and high dose NM-403, respectively

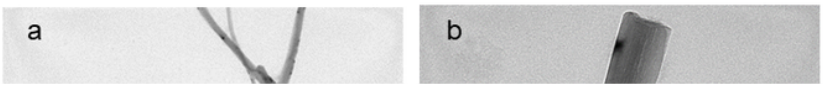

Figure 2

Transmission electron micrographs of NM-401 (a-b) and NM-403 (c-d), top and bottom panels, respectively, analyzed at 50,000x (left) and 150,000x magnifications (right)

Figure 3

Resonance Raman spectroscopy data of NM-401 and NM-403 in the frequency regions of 100–3200 cm^{-1}

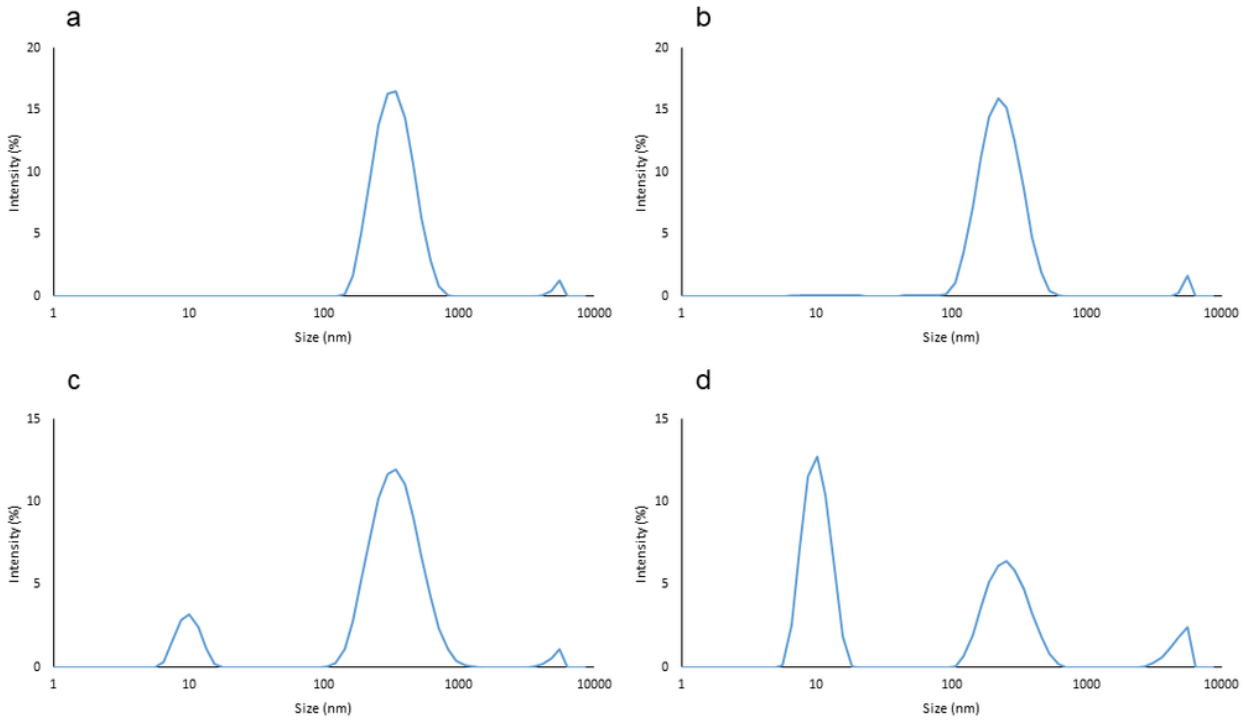

Figure 4

Hydrodynamic diameter characterization by dynamic light scattering analysis of NM-401 (a, b) and NM-403 (c, d) at low-dose (0.15 mg/ml, left panels) and high-dose (0.45 mg/ml, right panels) dispersions. Lines represent the mean of ten repeated reads performed for each preparation

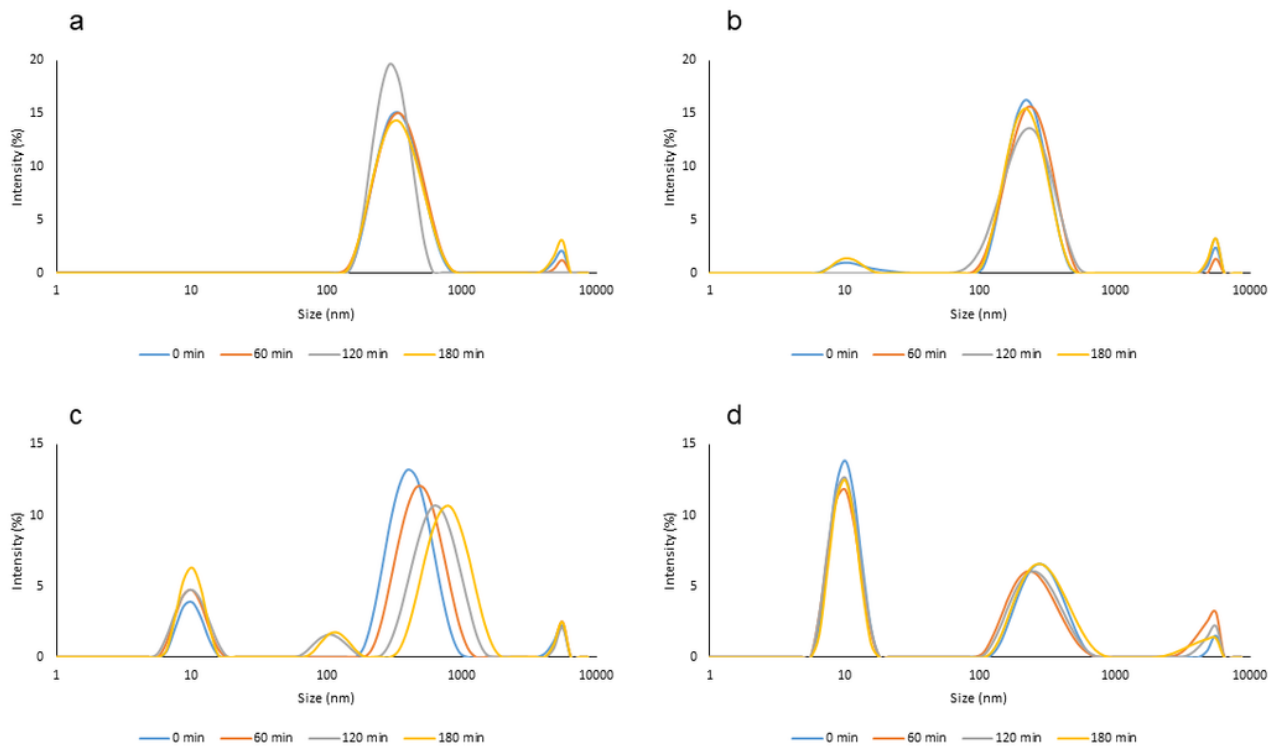

Figure 5

NM-401 and NM-403 stability study with reads at 0, 60, 120, and 180 minutes. Upper panels represent NM-401 at low concentration (0.15mg/ml, a) and high concentration (0.45mg/ml, b). Lower panels show NM-403 at low concentration (0.15mg/ml, c) and high concentration (0.45mg/ml, d)

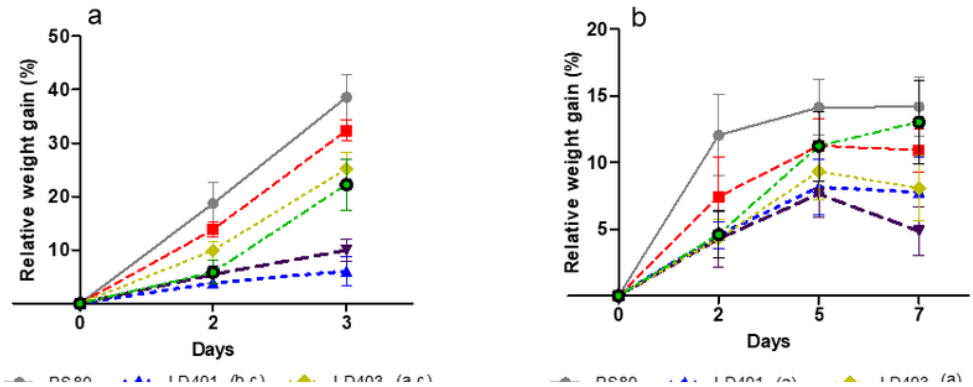

Figure 6

Relative body weight gain after the four different time points studied are shown in panels a, 3 days; b, 7 days; c, 30 days; and d, 90 days after the repeated MWCNT intratracheal administrations. Abbreviations: PS80: polysorbate 80 (0.1%) vehicle, ASB: asbestos crocidolite, LD401 and HD401: low dose and high dose NM-401, respectively, LD403 and HD403: low dose and high dose NM-403, respectively. For group lines, statistical signs in parenthesis represent (a) compared to PS80 ($P<0.05$, day 2); (b) compared to PS80 ($P<0.001$, day 2); (c) compared to PS80 ($P<0.001$, day 3); (d) compared to PS80 ($P<0.05$, day 7); (e) compared to PS80 ($P<0.001$, day 60); (f) compared to PS80 ($P<0.001$, day 90); (g) compared to ASB ($P<0.001$, day 60); and (h) compared to ASB ($P<0.001$, day 90). Data are presented as mean ± SEM (n = 6-8/group) and analyzed by two–way ANOVA/Bonferroni

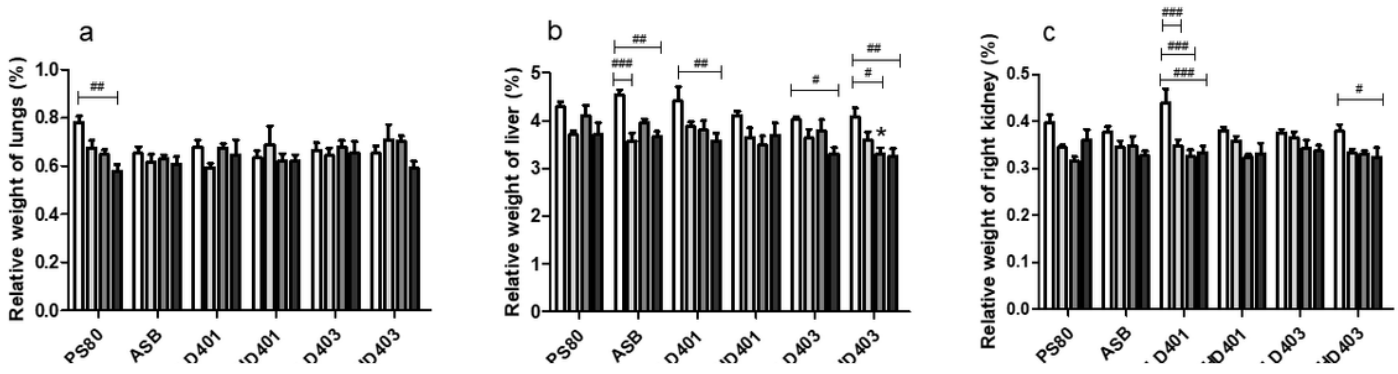

Figure 7

Relative weight of (a) lungs, (b) liver, (c) right kidney, (d) left kidney, (e) spleen, and (f) heart in the different time points after repeated administrations of both MWCNT. Abbreviations: PS80: polysorbate 80 (0.1%) vehicle, ASB: asbestos crocidolite, LD401 and HD401: low dose and high dose NM-401, respectively, LD403 and HD403: low dose and high dose NM-403, respectively. Data are presented as mean ± SEM (n = 6-8/group). * P<0.05 compared to PS80 (one-way ANOVA/Bonferroni); #P<0.05, ##P<0.01, and ###P<0.001 (two-way ANOVA/Bonferroni)

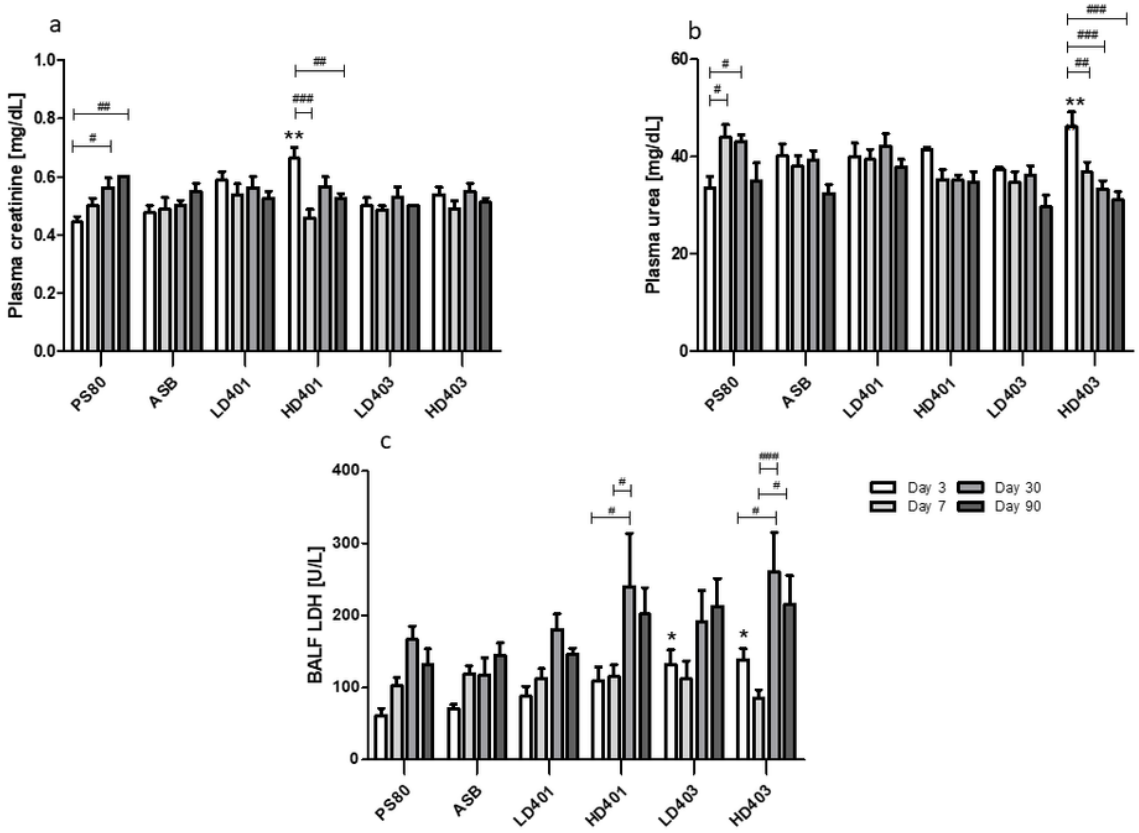

Figure 8

Biochemical alterations in MWCNT-administered rats at the time points evaluated. a, plasma urea levels; b, creatinine levels measured in plasma; and c, lactate dehydrogenase (LDH) levels measured in BALF. Abbreviations: PS80: polysorbate 80 (0.1%) vehicle, ASB: asbestos crocidolite, LD401 and HD401: low dose and high dose NM-401, respectively, LD403 and HD403: low dose and high dose NM-403, respectively. Data are presented as mean ± SEM (n = 6-8/group). *P<0.05 compared to PS80 and **P<0.01 compared to PS80 (one-way ANOVA/Bonferroni); #P<0.05, ##P<0.01, and ###P<0.001 (two-way ANOVA/Bonferroni)

Figure 9

Histopathological analysis of lung tissues sections stained with hematoxylin and eosin (H&E). Representative micrographs of pulmonary findings showing: a, bronchus-associated lymphoid tissue (BALT) in PS80; b-c, alveolar septal thickening (AST), granuloma, fibrosis, hemorrhagic foci, and black dots in alveoli and bronchioles in HD401; d, AST, hemorrhagic foci, fibrosis and perivascular granuloma in asbestos crocidolite; and e-f, AST, granuloma, fibrosis and hemorrhagic foci in HD403 (n=6-8/group). a, b, d, e (20x magnifications) and c, f (40x magnifications)

Figure 10

Histopathological analysis of extrapulmonary tissues (liver, kidney and spleen) stained with hematoxylin and eosin (H&E). Liver (panels a, d) and renal (panels b, c, e) tissue section micrographs demonstrate single occurencies – a, Kupffer cells with dark dots in LD401 after 7 days; b, glomerular and tubulointersticial congestion, and hyperemia in LD401 after 7 days; c, dark dots in blood vessels and tubular intersticial tissue in HD401 after 30 days; d, focal portal granuloma in HD403 after 30 days; e, congested glomerules, intersticial granuloma foci in cortical and medular areas, intratubular granuloma, and presence of hyaline deposition in tubules after 90 days in LD401; and f, spleen macrophages containing dark dots in LD401 after 7 days were also observed in asbestos, NM-401 and NM-403 groups (n=6-8/group). a, b, c, f (20x magnifications) and d, e (40x magnifications)

Supplementary Files

This is a list of supplementary files associated with this preprint. Click to download.

- BubolsSupplementarymaterial.pdf